Available online at www.sciencedirect.com
ScienceDirect
Journal of Nuclear Materials 363–365 (2007) 211–215
journal of nuclear materials
www.elsevier.com/locate/jnucmat

Modeling of multi-dimensional impurity transport in a realistic tokamak geometry

A. Fukano [a,*], M. Noritake [b], K. Hoshino [b], R. Yamazaki [b], A. Hatayama [b]

[a] *Monozukuri Department, Tokyo Metropolitan College of Industrial Technology, Higashi-Ohi, Shinagawa, Tokyo 140-0011, Japan*
[b] *Faculty of Science and Technology, Keio University, Yokohama 223-8522, Japan*

Abstract

A 3D Monte Carlo transport code of heavy metal impurities is developed. The code includes most of important processes of heavy metal impurities, such as Larmor gyration, friction force, Coulomb collision, multi-step ionization and recombination process. The code outputs the 2D density profiles of tungsten impurity on realistic tokamak geometry. Calculations are made for given background plasma profiles for attached and detached plasma, which are the typical conditions in front of the divertor plate. In the attached plasma state, impurity tungsten particles are ionized to higher charge states near the divertor plate due to high background plasma electron temperature. On the other hand, in the detached plasma state, ions in higher charge states exist in the upstream of the divertor region mainly due to low background plasma electron temperature in front of the target plate. Although the code is still under development, it well describes the qualitative feature of impurity transport in the realistic tokamak geometry.

PACS: 52.20.Hv; 52.25.Vy; 52.40.Hf; 52.65.Pp

Keywords: Impurity transport; Monte Carlo method; Divertor region; Detached plasma; Tungsten

1. Introduction

Reducing particle and heat loads on the divertor plate is one of the most important issues to realize magnetic confinement fusion using a tokamak device. Various simulation models for impurity behavior [1–5] and for plasma flow [6–8] have been developed, and contribute to understand the underlying physics. Recent year, tungsten has been paid attention as a divertor plate material which is not subjected to chemical sputtering [9,10]. On the other hand, however, the atomic number and charge number of tungsten are so high that radiation cooling of main plasma may occur even if small amount of tungsten enters to the main plasma. Therefore, it is very important to understand the transport process of tungsten impurities ions in the SOL/divertor region and to estimate the amount of impurities that enter to the main plasma. Since the Larmor radius of heavy ions is large and its mean free path is short, in order to analyze heavy impurity ions, such as

* Corresponding author. Address: 1-10-40 Higashi-Ohi, Shinagawa-ku, Tokyo 140-0011, Japan. Fax: +81 3 3471 6338.
E-mail addresses: fukano@tokyo-tmct.ac.jp (A. Fukano), khoshino@ppl.appi.keio.ac.jp (K. Hoshino).

0022-3115/$ - see front matter
doi:10.1016/j.jnucmat.2007.01.037

tungsten, not only the motion of the guiding center along the magnetic field line, but also the gyro-motion must be considered. We have developed the 3D Monte Carlo transport code for analysis of heavy impurity and calculated density profile for tungsten ions in a simple slab geometry [11].

In this article, we improve the code to apply the realistic tokamak geometry and present the preliminary calculation results. The code includes most of important processes of heavy metal impurities, such as Larmor gyration, friction force, Coulomb collision, multi-step ionization and recombination processes. In order to take into account the effect of the gyro-motion, 3D equations of motion are solved directly by this code, not using the guiding center approximation.

2. Transport of impurity

2.1. Transport of neutral impurity particles

Impurity particles are sputtered from the divertor plate by charge exchange neutral particles and self-sputtering. A test particle is launched by the assumed initial velocity and angle from the divertor plate. The simulation code traces the neutral impurity trajectory until the particles to be ionized or reach to the calculation boundary. The computational region is divided into small cells and the ionized point is determined by $\int_0^{L_{\text{ion}}} \mathrm{d}s/\lambda(s) = -\ln \xi_1$, where L_{ion} is the ionization length, $\lambda(s)$ is the local mean free path at the position s and ξ_1 $(0 \leqslant \xi_1 \leqslant 1)$ is a uniform random number. The density of neutral particle at each cell is determined by the method of path length estimator [12].

2.2. Transport of impurity ions

The trajectories of impurity ions are traced from the equation of motion

$$m\frac{\mathrm{d}v}{\mathrm{d}t} = Ze(\boldsymbol{E} + v \times \boldsymbol{B}) + (\text{Coulomb collision}) + (\text{multi-step ionization and recombination}), \quad (1)$$

where m is the impurity mass, v is the velocity and Z is the charge number of impurity ion, $\boldsymbol{E}$ and $\boldsymbol{B}$ are the electric field and magnetic field, respectively. The code uses the leap flog method to solve Eq. (1). In order to consider a collision between the impurity ion and the background plasma, we take into account the Coulomb collision by binary collision method (BCM) [13]. The velocity of a background plasma ion due to the binary collision with a test impurity ion is sampled from a shifted Maxwellian velocity distribution with a local plasma temperature and a local flow velocity parallel to the magnetic field. The scattering angles θ and φ in a time step Δt in the center of mass system are randomly chosen by means of the Monte Carlo method. The scattering angles are given by θ $2\arctan\xi_2$ and φ $2\pi\xi_3$, respectively. Here ξ_2 is a random number chosen from Gaussian distribution $\langle\xi_2\rangle = 0$ and $\langle\xi_2^2\rangle = \left[q_{\text{H}}^2 q_{\text{W}}^2 n_{\text{H}} \ln \Lambda/\left(8\pi\varepsilon_0^2 m_{\text{r}}^2 u^3\right)\right]\Delta t$, where q_{H} is the charge of hydrogen, q_{W} is the charge of tungsten, n_{H} is the hydrogen density, ε_0 is the dielectric coefficient of vacuum, m_{r} is the reduced mass, u is the relative velocity between the impurity ion and hydrogen ion and Δt is the time step, and ξ_3 $(0 \leqslant \xi_3 \leqslant 1)$ is a uniform random number.

We take into account the multi-step ionization and recombination processes of the impurity ions. Since a simple Monte Carlo method takes long calculation time, an implicit Monte Carlo method [14] is used. The transition probability of the multi-step

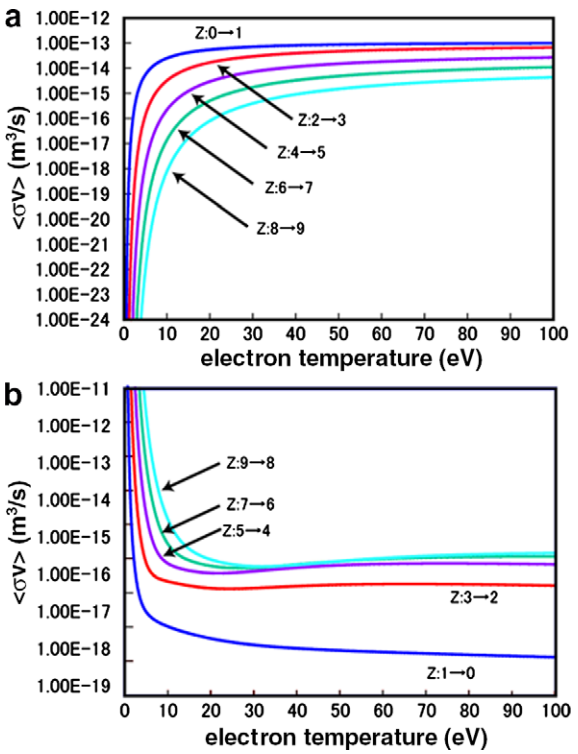

Fig. 1. Reaction rate coefficients for tungsten: (a) ionization rate coefficient and (b) recombination rate coefficient (cited from Ref. [10]).

ionization and recombination is given by the plasma temperature and density. The transition probability from the kth charge state to the k'th charge state between a time step Δt is obtained by solving the rate equations for each charge state and defined by $P_{k\to k'}(\Delta t) = n_k(t+\Delta t)/n_{k'}(t+\Delta t)$, where n_k is the impurity density of the charge number Z_k and $n_{k'}$ is the impurity density of the charge number $Z_{k'}$. The transition of charge state for impurity ions is determined by these transition probabilities and a uniform random number ξ_4. If $\sum_{i=0}^{k'-1} P_{k\to i}(\Delta t) \leqslant \xi_4 \leqslant \sum_{i=0}^{k'} P_{k\to i}(\Delta t)$, impurity ion of the charge number Z_k is considered to be transited to the charge number $Z_{k'}$. The density of impurity ions for each charge state at each cell is obtained by the same method as that for the neutral particles. The reaction rate coefficients of ionization and recombination for tungsten calculated from Ref. [15] are shown in Fig. 1.

3. Preliminary simulation results

In order to consider effect of tokamak geometry, magnetic field profile needs to be calculated and the calculation region needs to be divided into small meshes in which the magnetic field strength is almost constant. In calculations of magnetic field and mesh geometry, Carre code [16] is used. The mesh geometry generated from JT-60U MHD equilibrium and used in the present code is shown in Fig. 2.

Simulations are made for both the attachment plasma and the detachment plasma, which are the typical situations of the divertor plasma. To study qualitative behavior of the impurity particles, the neutral particles are uniformly generated from the divertor plate with monotonic energy. The background plasma profiles used in the calculation are given from the results of the background fluid plasma code (B2–EIRENE) [8] and shown in Fig. 3.

Relative density profiles of neutrals and relative total density profiles of tungsten ions for each charge state are shown in Fig. 4. Here the relative density is defined as the density normalized by a weight per a test particle. This is expressed by $\tilde{n}_{ik} = n_{ik}/(F/N) = [F\Delta t_{ik}/(N\Delta V_i)]/(F/N) = \Delta t_{ik}/\Delta V_i$, where F is the number of generated impurity neutrals per second, N is the number of test particles, Δt_{ik} is the time taken for particles in kth charge state to traverse the ith cell, ΔV_i is the volume of ith cell and n_{ik} is the density of particles in kth charge

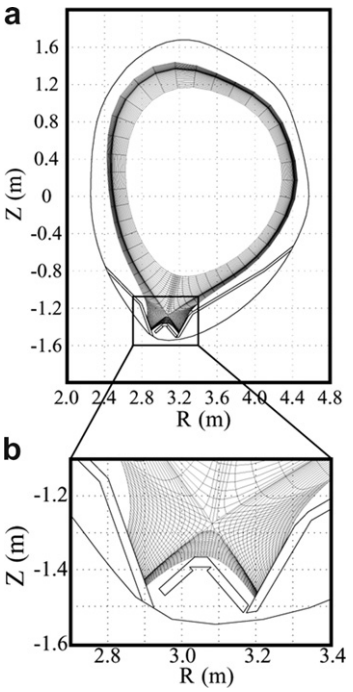

Fig. 2. Mesh geometry and its zoom-in view of the divertor region generated from JT-60U for numerical calculation.

state in the ith cell. Neutral particles widely distribute in the region where the background electron temperature is low. In addition, as the temperature is getting higher, particles are gradually ionized to higher charge states and transported towards the upstream in the divertor region. In the attached plasma state, impurity tungsten particles are ionized to higher charge states near the divertor plate due to high background plasma electron temperature. On the other hand, in the detached plasma state, ions in higher charge states exist in the upstream of the divertor region mainly due to low background plasma electron temperature in front of the target plate. This is shown more clearly by relative density profiles along the magnetic field for each charge state of tungsten in Fig. 5. These comparisons of the results for the attached plasma and detached plasma reasonably well describe the qualitative features of impurity transport. In the attached plasma state, since the collision time of ionization for each charge state particle is much shorter than that of recombination and the impurity ions are pushed back to the divertor plate by frictional force by the background plasma, the impurity particles in various charge states concentrate near the divertor plate. On the other hands, in the detached plasma

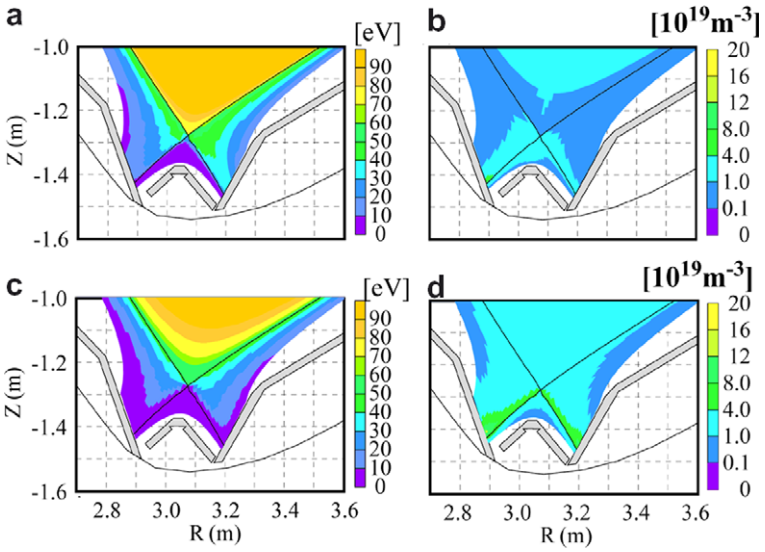

Fig. 3. Background plasma profiles of: (a) the electron temperature, (b) the electron density for the attached plasma, (c) and (d) are those for the detached plasma.

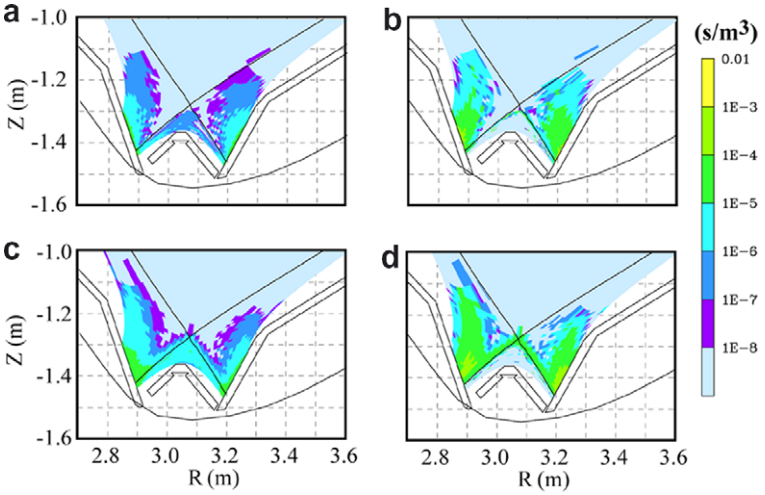

Fig. 4. Relative density profiles of: (a) neutral particle, (b) total of tungsten ions for each charge state for the attached plasma, (c) and (d) are those for the detached plasma.

state, since sink due to recombination becomes dominant for low charge state particles near the divertor plate, only impurity atoms exist near the divertor plate. Since time scale of ionization for the detached plasma state is much larger than that of the attached plasma state, impurity particles are transported far from the divertor plate before being multi-step ionized and position of the density peak extend to the upstream of the divertor region.

4. Summary and future plan

We have developed the 3D simulation code including various important processes for the heavy impurities for the realistic tokamak geometry. The 2D profiles of relative impurity density projected to the poloidal cross section in realistic tokamak geometry have been obtained. The results for attached plasma and detached plasma have been compared. As a result, effects of the background

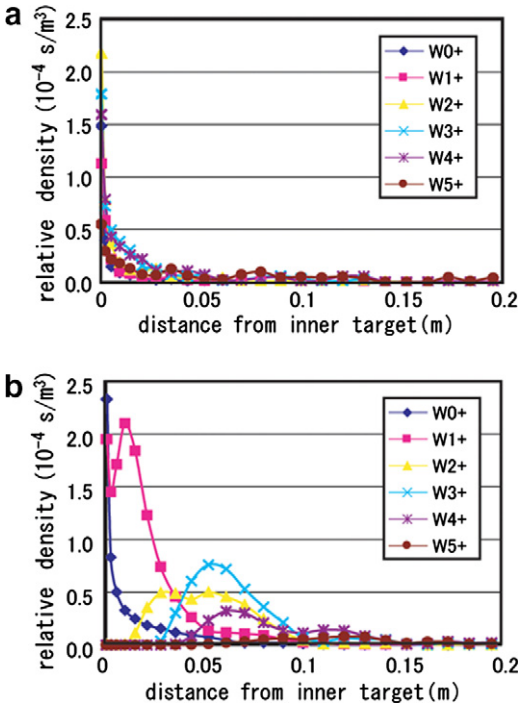

Fig. 5. Relative density profiles along the magnetic field at 30 mm outside from the separatrix on the inner divertor plate for each charge state: (a) for the attached plasma and (b) for the detached plasma.

plasma profiles on tungsten impurity were qualitatively confirmed.

The following will be refined for further improvement of the code: (1) impurity generation from the plate by the self-sputtering and the charge exchange neutral particles from the plasma, (2) the distributions of angle and energy of sputtered impurity particles, (3) the effect of prompt re-deposition, (4) connection with the background fluid plasma code, and (5) evaluation of the physical model by comparison with the experiment.

References

[1] S. Sengoku, M. Azumi, Y. Matsumoto, et al., Nucl. Fus. 19 (1979) 1327.
[2] J. Neuhauzer, W. Schneider, R. Wunderlich, et al., Nucl. Fus. 24 (1984) 39.
[3] D. Naujoks, R. Behrisch, J.P. Coad, et al., Nucl. Fus. 33 (1993) 581.
[4] R. Reiser, D. Reiter, M.Z. Tokar, Nucl. Fus. 38 (1998) 165.
[5] K. Ohya, R. Kawakami, T. Tanabe, et al., J. Nucl. Mater. 290–293 (2001) 303.
[6] A. Hatayama, H. Segawa, R. Schneider, et al., Nucl. Fus. 40 (12) (2000) 2009.
[7] K. Miyamoto, A. Hatayama, Y. Ishii, et al., J. Nucl. Mater. 313–316 (2003) 1036.
[8] K. Hoshino, A. Hatayama, R. Schneider, D.P. Coster, J. Nucl. Mater. 337–339 (2005) 276.
[9] G. Fussman et al. Proceeding of the 15th International Conference of Plasma Physics and Controlled Nuclear Fusion Research, vol. 2, IAEA, Vienna, 1995, p. 143.
[10] D. Naujoks, K. Asmussen, M. Bessenrodt-Weberpals, et al., Nucl. Fus. 36 (1996) 671.
[11] I. Hyodo, M. Hirano, K. Miyamoto, et al., J. Nucl. Mater. 313–316 (2003) 1183.
[12] M.H. Hughes, D.E. Post, J. Comp. Phys. 28 (1977) 43.
[13] T. Takizuka, H. Abe, J. Comp. Phys. 25 (1977) 205.
[14] A. Suzuki, T. Takizuka, K. Shimizu, et al., J. Comp. Phys. 131 (1997) 193.
[15] K. Asmussen et al., Nucl. Fus. 38 (1998) 967.
[16] R. Marchand et al., Comput. Phys. Commun. 96 (1996) 232.